T1 Mapping From MPRAGE Acquisitions: Application to the Measurement of the Concentration of Nanoparticles in Tumors for Theranostic Use

Audrey Lavielle, Fabien Boux, Justine Deborne, Noël Pinaud, Sandrine Dufort, Camille Verry, Sylvie Grand, Irène Troprès, Clément Vecco-garda, Géraldine Le Duc, et al.

RESEARCH ARTICLE

T_1 Mapping From MPRAGE Acquisitions: Application to the Measurement of the Concentration of Nanoparticles in Tumors for Theranostic Use

Audrey Lavielle, MSc,[1] Fabien Boux, PhD,[2] Justine Deborne, PhD,[1] Noël Pinaud, BS,[1] Sandrine Dufort, PhD,[2] Camille Verry, MD, PhD,[3] Sylvie Grand, MD, PhD,[3] Irène Troprès, PhD,[4] Clément Vecco-Garda, PhD,[5] Géraldine Le Duc, PhD,[2] Stéphane Mornet, PhD,[5] and Yannick Crémillieux, PhD[1]*

Background: The measurement of the concentration of theranostic agents in vivo is essential for the assessment of their therapeutic efficacy and their safety regarding healthy tissue. To this end, there is a need for quantitative T_1 measurements that can be obtained as part of a standard clinical imaging protocol applied to tumor patients.
Purpose: To generate T_1 maps from MR images obtained with the magnetization-prepared rapid gradient echo (MPRAGE) sequence. To evaluate the feasibility of the proposed approach on phantoms, animal and patients with brain metastases.
Study Type: Pilot.
Phantom/Animal model/Population: Solutions containing contrast agents (chelated Gd^{3+} and iron nanoparticles), male rat of Wistar strain, three patients with brain metastases.
Field Strength/Sequence: A 3-T and 7-T, saturation recovery (SR), and MPRAGE sequences.
Assessment: The MPRAGE T_1 measurement was compared to the reference SR method on phantoms and rat brain at 7-T. The robustness of the in vivo method was evaluated by studying the impact of misestimates of tissue proton density. Concentrations of Gd-based theranostic agents were measured at 3-T in gray matter and metastases in patients recruited in NanoRad clinical trial.
Statistical Tests: A linear model was used to characterize the relation between T_1 measurements from the MPRAGE and the SR acquisitions obtained in vitro at 7-T.
Results: The slope of the linear model was 0.966 ($R^2 = 0.9934$). MPRAGE-based T_1 values measured in the rat brain were 1723 msec in the thalamus. MPRAGE-based T_1 values measured in patients in white matter and gray matter amounted to 747 msec and 1690 msec. Mean concentration values of Gd^{3+} in metastases were 61.47 µmol.
Data Conclusion: The T_1 values obtained in vitro and in vivo support the validity of the proposed approach. The concentrations of Gd-based theranostic agents may be assessed in patients with metastases within a standard clinical imaging protocol using the MPRAGE sequence.
Evidence Level: 2.
Technical Efficacy: Stage 1.

J. MAGN. RESON. IMAGING 2022.

View this article online at wileyonlinelibrary.com. DOI: 10.1002/jmri.28509

Received Jul 8, 2022, Accepted for publication Oct 18, 2022.

*Address reprint requests to: Y.C., Institut des Sciences Moléculaires, Université de Bordeaux, 33076 Bordeaux, France.
E-mail: yannick.cremillieux@u-bordeaux.fr

From the [1]Institut des Sciences Moléculaires, UMR5255, Université de Bordeaux, France; [2]NH TherAguix SA, Meylan, France; [3]CHU Grenoble Alpes, Grenoble, France; [4]IRMaGe, CNRS, INSERM, Université Grenoble Alpes, CHU Grenoble, Grenoble, France; and [5]ICMCB, UMR 5026, Université de Bordeaux, France

The development and use of theranostic nanoparticles, defined as agents with coexisting therapeutic and imaging functions, offer the possibility of bringing diagnosis and therapy closer together.[1–3] Indeed, these nanosystems are expected to play an important role in personalized and precision medicine, with individualized therapies and optimized treatment approaches taking into account individual variability between patients. In the field of theranostic agents, MRI-traceable nanoparticles designed for preclinical and clinical applications represent a rapidly expanding area of research, which becomes apparent by the large and increasing number of publications: 36 and 221 articles were published, respectively, in 2011 and 2020, as revealed by a search associated with the topics "MRI theranostic agents" on WoS™.

The vast majority of these studies used paramagnetic (Gd^{3+} and Mn^{2+} ions) and iron-based superparamagnetic particles bound to the therapeutic part of the agent that can interact chemically or physically with the biological target (eg by heat or radiation).[4–10] In some cases, the MRI contrast agent is the therapeutic agent itself, as it is the case for gadolinium-based (Gd-based) radiosensitizing agents[11,12] or for iron magnetic particles inducing hyperthermia under an external alternating magnetic field.[13,14]

Regardless of the mechanism of action of these theranostic agents, measurement of their tissue concentration is necessary to assess their therapeutic efficacy and their safety regarding healthy tissue. Assuming that the longitudinal relaxivity (r_1) of these MRI theranostic agents is known, their concentration can be derived from the changes in T_1 values induced by their administration to the patient or the animal.[12,15,16] Several MRI sequences have been proposed to obtain quantitative T_1 maps in vivo. Although inversion recovery (IR) and saturation recovery (SR) sequences are considered the reference standard for generating T_1 maps,[17] in practice they are rarely used in vivo due to their relatively long acquisition times, which are hardly achievable with in vivo conditions.

Among the faster alternatives to IR and SR approaches for T_1 mapping are the look-locker (LL) sequences and the variable flip angle (VFA) technique.[18,19] Conventional three-dimensional (3D) LL sequences remain slow unless using echo-planar acquisitions, which comes at the cost of degraded spatial resolution and image quality.[17] The VFA method requires multiple spoiled gradient echo acquisitions and is known to be particularly sensitive to B_1 inhomogeneities.[20] More recently, based on an extension of the magnetization-prepared rapid gradient echo sequence (MPRAGE), the magnetization-prepared 2 rapid gradient echo (MP2RAGE) sequence has been proposed as a robust fast 3D T_1 mapping sequence with reduced sensitivity to B_1 inhomogeneities.[21]

However, in clinical practice constraints often arise regarding the content and the duration of the MRI protocol due to the individual patient health status, scanner occupancy rates, or the availability of imaging sequences, which limits the inclusion of T_1 mapping sequences in the image acquisition protocol. Regardless of these constraints, the response evaluation criteria in solid tumors (RECIST) guidelines have established standard imaging protocols to assess the treatment outcomes of solid tumors that are key endpoints in clinical trials.[22] When MRI is used to assess treatment response in such patients, anatomical 3D acquisitions combined with intravenous injection of Gd-based contrast agents are usually required in order to delineate the tumor and assess its size. For this purpose, the MPRAGE sequence, allowing strong T_1-weighting and rapid 3D coverage at isotropic high spatial resolution, is often part of the MRI protocol.

To take advantage of the frequent inclusion of the MPRAGE sequence in MRI protocols for patients with solid tumors, this study aimed first to evaluate the feasibility of producing T_1 maps from MPRAGE anatomical acquisitions and second to use these T_1 maps to image the concentration of potential theranostic nanoparticles in patients with brain metastases.

Materials and Methods

Studies were performed in accordance with the rules of the European Committee Council Directive 2010/63/EU after approval by our local animal welfare committee (University of Bordeaux, reference number 04490.02). All patients provided written informed consent in accordance with institutional guidelines.

Theoretical Approach

FROM MPRAGE IMAGE SIGNAL INTENSITY TO T_1 VALUES. In the MPRAGE sequence, an inversion pulse is applied in order to make the sequence sensitive to T_1 values during the recovery of the longitudinal magnetization. Following the inversion pulse, the longitudinal magnetization is repeatedly sampled using low flip angles, spatially encoded and acquired as a gradient echo.[23,24]

The analytical expression of the amplitude of each gradient echo signal in the echo train, once the steady state is reached, has been established and detailed in the literature.[23] Although the full expression of the signal amplitude appears rather complex, the signal amplitude depends on a limited number of sequence parameters (the inversion delay between the inversion and the readout pulses, the echo time [TE], the repetition time [TR], the number of readout pulses per inversion pulse, the position of the echo in the echo train, and the readout flip angle) as well as tissue nuclear magnetic resonance (NMR) properties such as T_1, T_2*, and proton density. In addition, the signal amplitude also depends on instrumentation factors related to the detection and amplification of the radiofrequency (RF) signal and to the strength of the magnetic field. Ignoring the image encoding phase gradients, the full analytical expression of the NMR signal amplitude for the MPRAGE sequence is represented by the following equations:

$$S_n = M_n \sin\theta e^{-\mathrm{TE}/T_2^*} \quad (1)$$

where S_n is the signal amplitude from the nth echo, M_n is the nuclear magnetization before the nth RF excitation pulse, θ is the

excitation flip angle, TE is the echo time, and T_2^* is the observed decay time. M_n is expressed as

$$M_n = M_0 \left[\frac{(1-\beta)\left(1-(\alpha\beta)^{n-1}\right)}{1-\alpha\beta} + (\alpha\beta)^{n-1}(1-\gamma) + \gamma(\alpha\beta)^{n-1}\frac{M_e}{M_0} \right] \quad (2)$$

with

$$\frac{M_e}{M_0} = -\left[\frac{1-\delta+\alpha\beta(1-\beta)\frac{1-(\alpha\beta)^{m-1}}{1-\alpha\beta}+\alpha\delta(\alpha\beta)^{m-1}-\alpha^m\rho}{1+\rho\alpha^m} \right] \quad (3)$$

using the following definitions: $\alpha = \cos\theta$, $\beta = e^{-T_b/T_1}$, $\gamma = e^{-T_a/T_1}$, $\delta = e^{-T_w/T_1}$, $\rho = e^{-TR/T_1}$, $T_w = \mathrm{TR} - T_a - (m-1)T_b$, where T_b is the time interval between two consecutive RF excitation pulses, T_a is the delay between the inversion pulse and the first RF excitation pulse, TR is the repetition time between two consecutive inversion pulses, m is the number of RF excitation pulses per inversion pulse, T_1 is the longitudinal relaxation time, and M_0 is the nuclear magnetization at thermal equilibrium. For all these equations, the integer n is comprised between 1 and m.

For a given set of MPRAGE acquisition parameters, the amplitude of each of the m echoes can be expressed as a function of the T_1 value. Among all the echoes acquired, the amplitude of the one corresponding to the center of the Fourier space is directly proportional to the image intensity. The measurement of the amplitude of the MPRAGE MRI signal in a region of interest (ROI) with a known T_1 value (eg an external reference or a tissue with well-established NMR properties) provides a pair (image intensity, T_1) of values. This pair of values is used to scale the plot of T_1 values as a function of the MRI signal amplitude. This results in a bijective correspondence between the MRI signal intensity and the T_1 values. Using this one-to-one correspondence for each pixel of the MPRAGE images, a 3D map of T_1 values can then be generated.

COMPUTATION OF T_1 MAPS AND CONTRAST AGENT CONCENTRATION MAPS. All computations, curves, simulations, processing, and image display presented in this study were done using MATLAB software (version 9.12; The Mathworks, Natick, MA, USA). Olea SDK software (version 1.5.3; Olea Medical, La Ciotat, France) was used for registration of images from precontrast and postcontrast acquisitions.

For in vitro MPRAGE acquisitions performed on solutions of contrast agents, the image intensity was measured in a ROI located in one of the contrast agent solutions. The pair of values (image intensity, T_1) in this ROI was used to scale the plot of T_1 values as a function of the MRI signal amplitude. The T_1 maps were generated assuming the same proton densities and T_2^* values in the whole MPRAGE images. For convenience, M_0 was set equal to 1 and $R_2^* = 1/T_2^*$ equal to zero.

For preclinical acquisitions, an external reference was used for scaling the T_1 vs. MRI signal intensity curves. The external reference was a solution of a Gd-based contrast agent, Dotarem® (Guerbet, Villepinte, France), at a concentration of 0.1 mM with a measured T_1 value of 1740 msec. The variations of proton density present in vivo were taken into account to generate the T_1 maps. Based on the literature,[25] proton density values ρ_{CSF} and ρ_{brain} were, respectively, set equal to 1 and 0.74 relative to the external reference. MRI signal intensities SI_{CSF} and SI_{brain} were measured in ROIs drawn in cerebrospinal fluid (CSF) and right cortex, respectively. Depending on its MRI signal intensity, each voxel of the MPRAGE image was then assigned a proton density value ρ, which was computed as follows:

$$\rho = \frac{|SI - SI_{CSF}|}{|SI_{brain} - SI_{CSF}|}\rho_{brain} + \frac{|SI - SI_{brain}|}{|SI_{brain} - SI_{CSF}|}\rho_{CSF}, \text{ for } SI_{CSF} < SI < SI_{brain} \quad (4)$$

$$\rho = \rho_{brain}, \text{ for } SI > SI_{brain} \quad (5)$$

$$\rho = \rho_{CSF}, \text{ for } SI < SI_{CSF} \quad (6)$$

Prior to the computation of the T_1 maps, the MRI signal intensity in each voxel was divided by its proton density, with the proton density in the external reference being set as one.

For human brain acquisitions, a pair of values (image intensity, T_1) in a ROI located in the occipital white matter (WM) was used to scale the plot of T_1 values as a function of the MRI signal amplitude. The T_1 value in the occipital WM was set to 830 msec according to the values reported in the literature.[26] The variations of proton density present in vivo in WM, gray matter (GM) and CSF were taken into account to generate the T_1 maps. The proton density values in WM, GM, and CSF used in this study were set equal respectively to $\rho_{WM} = 66\%$, $\rho_{GM} = 83\%$, and $\rho_{CSF} = 100\%$ of proton density of pure water at 37°C as reported in the literature.[25,26]

Average MRI signal intensities SI_{CSF}, SI_{GM}, and SI_{WM} were measured in ROIs corresponding to CSF, GM, and WM, respectively. ROIs were placed in the right lateral ventricle, occipital WM and occipital GM, by a researcher with more than 20 years of experience in MRI (Y.C.). Depending on the MRI signal intensity, each voxel of the MPRAGE images were then assigned a proton density value ρ, which was computed as follows:

$$\rho = \frac{|SI - SI_{GM}|}{|SI_{GM} - SI_{WM}|}\rho_{WM} + \frac{|SI - SI_{WM}|}{|SI_{GM} - SI_{WM}|}\rho_{GM}, \text{ for } SI_{GM} < SI < SI_{WM} \quad (7)$$

$$\rho = \frac{|SI - SI_{CSF}|}{|SI_{GM} - SI_{CSF}|}\rho_{GM} + \frac{|SI - SI_{GM}|}{|SI_{GM} - SI_{CSF}|}\rho_{CSF}, \text{ for } SI_{CSF} < SI < SI_{GM} \quad (8)$$

$$\rho = \rho_{WM}, \text{ for } SI > SI_{WM} \quad (9)$$

$$\rho = \rho_{CSF}, \text{ for } SI < SI_{CSF} \quad (10)$$

The ratio between the proton density value and that of the ROI in occipital WM used to normalize the T_1 curve as a function of the MRI signal intensity was calculated in each voxel to produce a proton density correction map. Before the computation of T_1 maps, the MRI signal intensity in each voxel was then divided by the proton density correction map.

To quantify the concentration of contrast agents in vivo, MPRAGE acquisitions performed before and after the administration of contrast agents were used. Image registration was performed between the precontrast and postcontrast MPRAGE images to correct for changes in subject position. A pair of values (image intensity, T_1) in a ROI located in the occipital GM was used to scale the plot of T_1 values as a function of the MRI signal amplitude. The T_1 value of GM was set to 1350 msec according to the values reported in the literature.[26] The proton density value was assumed not to be affected by the contrast agent administration. In each voxel, the concentration of the contrast agent was computed using the following formula:

$$\frac{1}{T_{1,post}} = \frac{1}{T_{1,pre}} + r_1 C \quad (11)$$

where $T_{1,pre}$ and $T_{1,post}$ are the T_1 values (in second unit) before and after the administration of the contrast agent, and r_1 is the longitudinal relaxivity of the contrast agents (in $mM^{-1}\ s^{-1}$).

EVALUATION OF ROBUSTNESS AND ACCURACY OF THE APPROACH. Numerical simulations were performed in order to estimate the relevance of approximations made and to evaluate the accuracy of the quantification of T_1 and contrast agent concentrations with respect to the uncertainties on some experimental values. These simulations were realized using a set of clinical MRI sequence parameters and acquisitions. They included assessment of the sensitivity of T_1 measurements in relation to the accuracy of proton densities. To this end, a multiplicative factor was applied to the proton density correction map. In each pixel, a numerical value was randomly generated from a zero-centered Gaussian distribution and the absolute value of the randomly generated number was used as a positive multiplier. The impact of the variation of T_2^* on the T_1 assessment was evaluated by using tissue T_2^* values and r_2^* relaxivity values from the literature, namely T_2^* values equal to 54 msec and 71 msec in the WM and GM, respectively[27] and r_2^* value of the chelated Gd ions equal to 19 $mM^{-1}\ s^{-1}$ at 3 T.[28]

MRI experiments

The in vitro and preclinical MRI experiments were performed on a 7-T scanner (BioSpec 70/20; Bruker Biospin, Ettlingen, Germany) with ParaVision software (version 6.0.1; Bruker, Biospin, Ettlingen, Germany). A quadrature Bruker volume coil with an 86-mm inner diameter was used. The clinical datasets were acquired at 3 T (Achieva, Philips Healthcare, Best, The Netherlands) using a 32-channel head coil.

IN VITRO MRI EXPERIMENTS. In vitro validation of the T_1 measurements obtained with the proposed approach was performed on solutions containing a Gd-based contrast agent Dotarem® and homemade ultra-small nanoparticles (USNP) of 4 ± 1 nm diameter maghemite iron oxide (γ-Fe_2O_3) cores synthesized according to a well-established procedure[29] and coated with low-molecular-weight polyethylene glycol macromolecules (1 kDa molecular weight) as previously described.[30] The Gd^{3+} concentrations in the eight Gd-based solutions were 0.01, 0.03, 0.05, 0.08, 0.1, 0.2, 0.3, and 0.4 mM. The iron concentrations in the eight USNP solutions were 0.05, 0.1, 0.15, 0.2, 0.3, 0.4, 0.5, and 0.6 mM.

Phantom images were acquired with the 3D modified driven equilibrium Fourier transform (MDEFT) sequence, equivalent to the MPRAGE sequence, with the following parameters: TE = 2.66 msec; TR = 2300 msec; inversion time (TI) = 1700 msec; flip angle α = 8°; bandwidth: 100 kHz; image size: 256 × 128 × 32; field of view (FOV) = 30 × 30 × 32 mm^3; spatial resolution: 0.11 × 0.23 × 1 mm^3; number of averages: 20; total acquisition time: 24 minutes 32 seconds.

A SR sequence was also applied on the same phantoms. The acquisition parameters were TE = 5.9 msec; TR = 100/200/400/1000/8000/13000 msec; flip angle α = 90°; bandwidth: 100 kHz; image size: 128 × 128; FOV = 30 × 30 mm^2; slice thickness: 1 mm; spatial resolution 0.23 × 0.23 mm^2; number of averages: 4; acquisition time: 1 hour 36 minutes 51 seconds. The SR-based T_1 maps were generated using the ParaVision software.

For the Gd-based phantom, the image intensity was measured in a ROI located in the solution with 0.3 mM Gd^{3+} concentration. For the USNP-based phantom, the image intensity was measured in a ROI located in the solution with 0.5 mM iron concentration. The T_1 values in these two solutions were measured using the SR sequence. The resulting pair of values (image intensity, T_1) were used for scaling the plot of T_1 values, derived from the MPRAGE acquisition, as a function of the MPRAGE MRI signal amplitude. T_1 values in the MPRAGE-derived and the SR-derived T_1 maps were measured in circular ROIs positioned in the center of each tube containing the contrast agent solutions.

IN VIVO PRECLINICAL MRI EXPERIMENTS. Male rat of Wistar strain was used for an in vivo proof of concept. The animal was procured from the Janvier Laboratory (Le Genest-Saint-Isle, France). It was kept in standard housing conditions (12 hours light–dark cycles) with a standard rodent chow and water available ad libitum.

Rat brain images were acquired using the MDEFT sequence, with the following parameters: TE = 3.94 msec; TR = 2300 msec; TI = 1700 msec; flip angle α = 8°; bandwidth: 50 kHz; image size: 256 × 128 × 32; FOV = 40 × 40 × 22 mm^3; spatial resolution: 0.15 × 0.31 × 0.67 mm^3; number of averages: 10; total acquisition time: 12 minutes 16 seconds.

A SR sequence was also used for scanning the animal. The acquisition parameters were TE = 6.5 msec; TR = 100/200/400/1000/2000/10000 msec; flip angle α = 90°; bandwidth: 78 kHz; image size: 128 × 128; FOV = 40 × 40 mm^2; slice thickness: 1 mm; spatial resolution: 0.31 × 0.31 mm^2; number of averages: 2; acquisition time: 29 minutes 13 seconds. The SR-based T_1 maps were generated using the ParaVision software.

CLINICAL MRI DATASET. The clinical MPRAGE images used in this study were issued from the Radiosensitization of Multiple Brain Metastases Using AGuIX Gadolinium Based Nanoparticles (NanoRad, NCT02820454) trial, which was completed in February 2019.[6] NanoRad was a prospective dose escalation phase Ib clinical trial to evaluate the tolerance of the intravenous administration of radiosensitizing Gd-based nanoparticles[31] in combination with whole brain radiotherapy for the treatment of brain metastases. The three patients of the clinical trial who received an intravenous injection of nanoparticles at 100 mg/kg body weight were considered in this study. The sex, age, and primary tumor type of patient #1, #2, and #3 were, respectively, 58-years-old female, lung cancer; 46-years-old male, lung cancer; 61-years-old female, breast cancer. The r_1 value of this theranostic agent (AGuIX, NH TherAguix, Meylan, France) was measured equal to 8.9 mM^{-1} s^{-1} per Gd^{3+} ion at 3 T. Detailed information on the NanoRad trial can be found in previous literature.[6,12]

The MPRAGE datasets were acquired in patients, before and after the administration of the Gd-based theranostic agents with the following sequence parameters: T_b/TE = 8.3/3.8 msec, T_a = 260.9 msec, TR = 2.375 seconds, number of RF excitation pulses per inversion pulse m = 154, center of Fourier space acquired for the 77th excitation pulse, flip angle $\alpha = 8°$, FOV = 256 × 256 × 220 mm^3, acquisition matrix: 256 × 256 × 220, resolution: 1 × 1 × 1 mm^3, total acquisition time: 4 minutes 39 seconds.

For each of the three patients, ROIs, excluding necrotic parts, were manually drawn on the concentration map on all metastases larger than 1 cm in diameter by senior researcher (Y.C.). The mean and SD of the concentration values were computed for each of these ROIs.

Statistical analysis

Linear regression between MPRAGE and SR measurements of T_1 values in vitro at 7 T was done using MATLAB software (version 9.12; The Mathworks, Natick, MA, USA). A linear model (without intercept) was used to characterize the relationship between the T_1 measurements obtained from the MPRAGE and the SR acquisitions. Coefficient of determination R^2 was used to assess how well this linear model fit the data.

Results

Computation of T_1 Maps

Based on the MPRAGE sequence parameters used in the NanoRad clinical trial and using Eqs. 1–3, the T_1 value plotted as a function of the amplitude of the echo acquired at the center of the Fourier space is shown in Fig. 1a and the curve of T_1 vs. MRI signal is shown in Fig. 1b. For this specific example from patient #1, the MPRAGE signal intensity measured in the occipital WM was equal to 1377 (arbitrary unit).

Figure 2 illustrates for the same patient the transition between an MPRAGE image (Fig. 2a) and the corresponding computed T_1 map (Fig. 2b). The proton density correction map is shown in Fig. 2c.

In Vitro MRI Experiments

T_1 maps obtained with the reference SR technique and the proposed MPRAGE-based approach are shown in Fig. 3 for Gd-based contrast agents (Fig. 3a,b) and USNP solutions (Fig. 3c,d).

With the concentration range of contrast agents used, T_1 values varied from 500 msec to 3000 msec. The T_1 values obtained with the MPRAGE acquisitions as a function of the reference SR-derived T_1 values are shown in Fig. 4. The plots and linear regressions showed an excellent match between the results obtained with the two techniques, slopes were equal to 0.966 (R^2 = 0.9934) and 0.927 (R^2 = 0.9813) for Gd-based and USNP contrast agents, respectively.

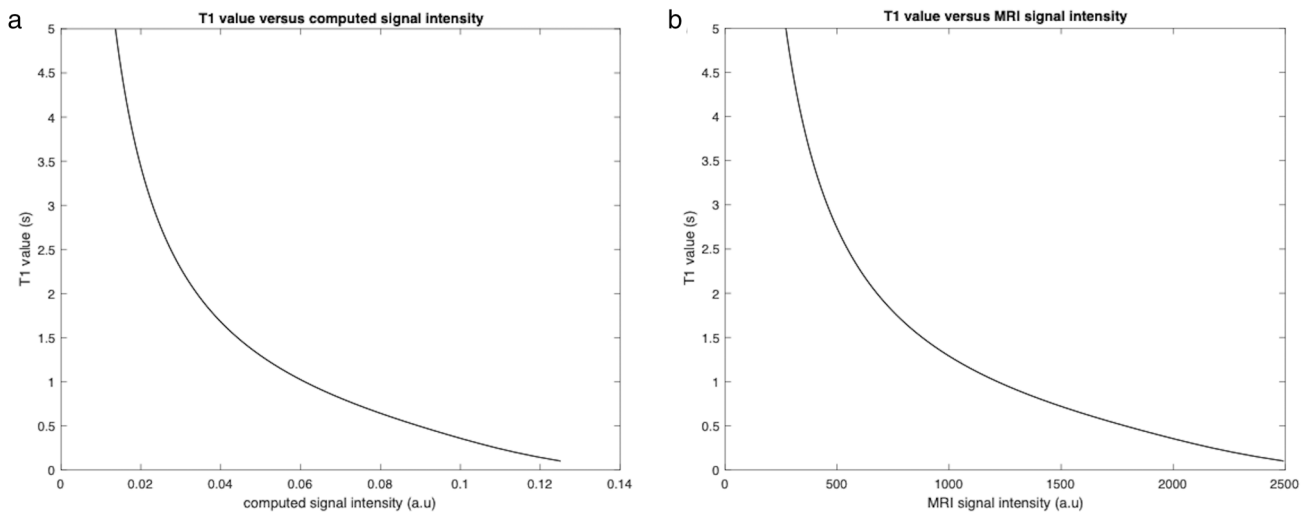

FIGURE 1: (a) T_1 value plotted as a function of computed signal intensity. The signal intensity for the central echo in the Fourier space, n = 77, was computed using Eq. 1–3 with the following acquisitions parameters: $\theta = 8°$, T_b = 8.3 msec, T_a = 260.9 msec, TR = 2.375 seconds, T_w = 205.1 msec, m = 154 excitation pulses per inversion pulse and T_1 varying between 100 and 5000 msec. (b) T_1 value plotted as a function of the MRI signal intensity in the MPRAGE image after scaling of the curve with a pair of (image intensity = 1377, T_1 = 830 msec values measured in occipital GM of patient #1.

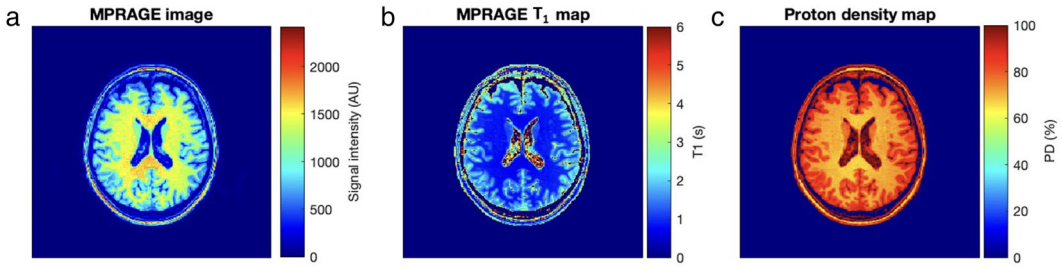

FIGURE 2: (a) MPRAGE image acquired at 3 T in the patient #1 with the same sequence parameters as those used in the signal intensity computation shown in Fig. 1a. (b) T_1 map derived from the MRI image intensity of Fig. 1a using correction of proton density in WM, GM, and CSF. (c) The corresponding proton density correction map applied to the MPRAGE image before the T_1 map is computed.

In Vivo Preclinical MRI Experiments

A slice extracted from the 3D MPRAGE dataset acquired on rat brain is shown in Fig. 5a. The external tube corresponded to a solution of Gd-based contrast agent with a measured T_1 value of 1740 msec. A resulting MPRAGE-derived T_1 map is shown in Fig. 5b and the corresponding reference SR T_1 map in Fig. 5c. The spatial resolution of the T_1 maps was identical to the corresponding MPRAGE and SR images, namely $0.15 \times 0.31 \times 0.67\ mm^3$ for the MPRAGE-derived map and $0.31 \times 0.31 \times 1\ mm^3$ for the SR-derived map.

The T_1 values obtained from ROIs drawn in different brain regions are summarized in Table 1, including also typical T_1 values reported in the literature.[32] As a point of comparison, the T_1 values that were obtained without correcting for the proton density in the thalamus, cortex, and hippocampus amounted to 2356 ± 135 msec, 2676 ± 175 msec, and 2535 ± 155 msec, respectively.

Processing of Clinical MRI Data and Evaluation of the Measurement Robustness

The histogram of T_1 values in the T_1 map displayed in Fig. 2b is shown in Fig. 6a. T_1 values ranged between 0.36 seconds and 6 seconds. A bimodal distribution is noticeable with a narrow peak of values centered on 0.88 seconds

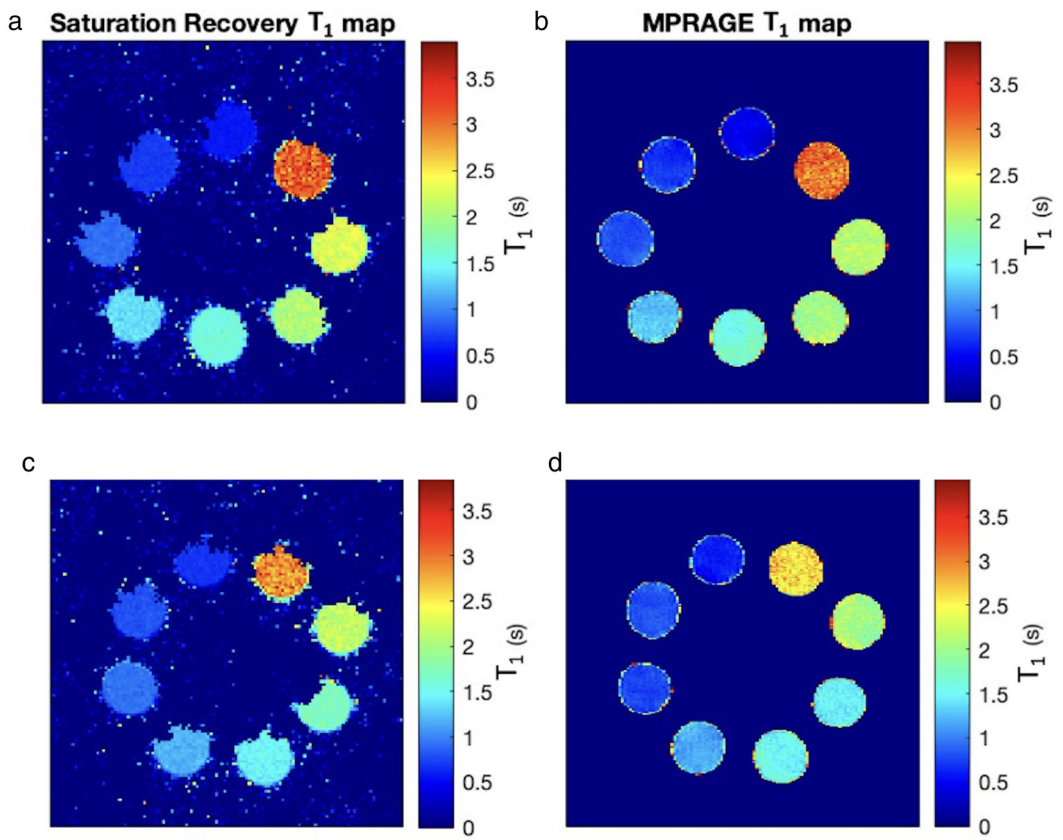

FIGURE 3: T_1 maps of solutions of Gd-based contrast agents obtained at 7 T (a) with the reference SR sequence and (b) from the MPRAGE acquisition. T_1 maps of solutions of USNP obtained at 7 T (c) with the reference SR sequence and (d) from the MPRAGE acquisition. The top tube corresponds to the highest concentration of contrast agents (Gd-based and USNP). The concentration of contrast agent in the tubes decreases counter-clockwise.

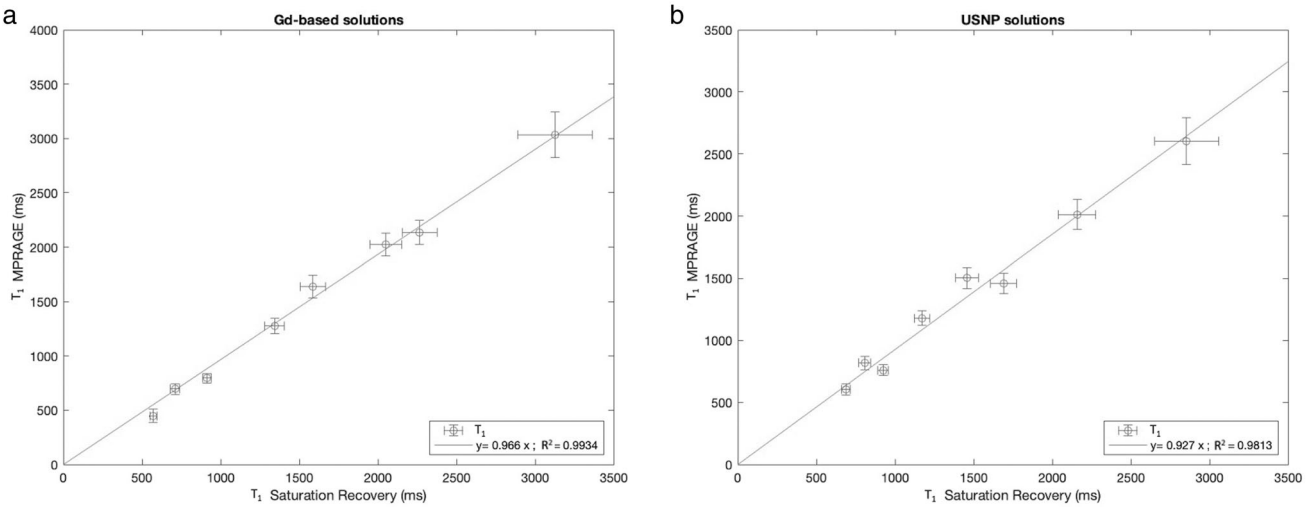

FIGURE 4: MPRAGE-derived T_1 values as a function of reference SR-derived T1 values. Each point corresponds to the mean measured T_1 value in a solution with a given contrast agent concentration. Vertical and horizontal error bars correspond to standard deviations on the T_1 values. Black lines correspond to the linear regressions. T_1 measurements performed (a) on Gd-based solutions and (b) on USNP solutions.

and a broader peak centered at 1.76 seconds. The tail of the distribution shows a slow increase of T_1 value culminating at 5.96 seconds. The T_1 values from the narrow peak can be attributed to the WM brain regions, while the broader peak corresponds to the GM tissue and the higher T_1 values to the CSF. The mean and the standard deviation of T_1 values measured in the occipital WM and occipital GM for the patients #1, #2 and #3 were, respectively, 0.747 ± 0.051 and 1.690 ± 0.118 seconds.

The impact of inaccurate proton density values on the histogram of T_1 values is shown in Fig. 6b–d, with increasing Gaussian variance of the randomly generated multiplier. An increase of T_1 values with increasing SD of the Gaussian distribution can be noticed from the peaks corresponding to the WM and GM. The maximum peak amplitudes corresponding to the T_1 value from WM were 0.920, 0.960, 1 second and for the T_1 value from GM were 1.800, 1.880, 1.920 seconds for the standard deviation of 10%, 20%, and 30%, respectively. A broadening of the two peaks with increasing SDs can be noticed from the histograms. The mean and SD of T_1 values measured in regions corresponding to WM and GM tissue varied from 0.858 ± 0.060 and 1.642 ± 0.121 seconds in the original T_1 map to 0.943 ± 0.084, 1.001 ± 0.125, 1.059 ± 0.153 seconds and 1.743 ± 0.131, 1.814 ± 0.224, 1.904 ± 0.277 seconds with SDs equal to 10%, 20%, and 30%, respectively.

Based on the 3.8 msec TE used in the clinical MPRAGE sequences and on the T_2^* relaxation values in brain,[28] the T_2^* relaxation resulted in an MRI signal intensity decrease of 6.8% and 5.2% in WM and GM, respectively, and in a difference in signal intensity variations between these two tissues that was equal to 1.6%.

Computation of the Concentration of Theranostic Agents in Brain Metastases

Examples of MPRAGE images acquired in patient #1 pre- and post-injection of theranostic agents and the corresponding derived T_1 maps are shown in Fig. 7. The uptake of contrast agents in the MPRAGE images is clearly visible in two brain metastases located in the right and left temporal lobes. Changes in metastases T_1 values following the administration of the theranostic agent is readily visible 2 hours after the injection.

Examples of concentration maps obtained in each of the three patients and computed using Eq. 11 are shown in Fig. 8. For the specific concentration map of patient #1, the

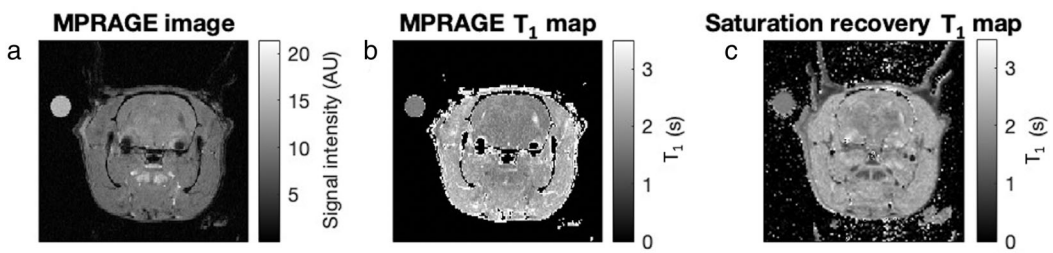

FIGURE 5: (a) Slice extracted from a 3D MPRAGE data set acquired in a rat brain. (b) Corresponding T_1 map derived from the MPRAGE acquisition. (c) T_1 map obtained with a reference SR sequence at the same slice position.

TABLE 1. Mean and SD of T_1 Values Obtained From the Reference SR and MPRAGE Sequence

	SR-Derived T_1	MPRAGE-Derived T_1	T_1 Literature Value[32]
Thalamus	1896 ± 127 msec	1723 ± 166 msec	1500–1650 msec
Cortex	2354 ± 204 msec	1908 ± 130 msec	1750–1900 msec
Hippocampus	2281 ± 185 msec	1984 ± 203 msec	1800–1950 msec

The last column contains typical values in rat brain regions reported in the literature.[32]

mean and SD of Gd^{3+} concentrations in the left and right metastases were equal to 78.5 ± 18.6 and 97.2 ± 15.5 μM, respectively, with the concentration values in the latter ranging from 46.4 to 118.3 μM. The artefactual concentration values noticeable at the interface between brain structures are obviously due to imperfection in the image registration and to small nonrigid displacements. The mean Gd^{3+} concentrations in all metastases larger than 1 cm in diameter and in the occipital GM are given for each patient in Table 2.

Discussion

In this work, we demonstrated the possibility of deriving T_1 maps from MPRAGE acquisitions. The accuracy and robustness of the approach was evaluated in vitro in phantoms, on a small animal and in patients. From MPRAGE acquisitions performed in a clinical research protocol following RECIST recommendations, we demonstrated the possibility to assess the concentration of Gd-based nanoparticles in brain metastases of patients.

The T_1 measurements obtained in vitro on contrast agent solutions (Gd-based and USNP) indicate that the proposed approach and the algorithm used in this study are valid and robust for in vitro measurements. They provided results comparable to what is obtained with reference T_1 measurement techniques such as the SR sequence. It should be noted that the acquisition times were four times shorter with the 3D MPRAGE acquisition than with the single-slice SR sequence The choice of concentration ranges for this in vitro evaluation was made to cover a wide range of T_1 values from 0.5 to 3 seconds, corresponding to values found in brain tissue (excluding CSF) without and in the presence of contrast agents.

The consideration of proton density variations included in the proposed approach was evaluated on the healthy rat brain. The density correction performed for the brain tissue provided values close to the literature values with a differentiation of the thalamus from the cortex or hippocampus.[32] The elevated values obtained without density correction illustrate the importance of density correction when an external reference is used. As with the in vitro measurements, the T_1 maps obtained from the MPRAGE sequence illustrate the potential of the approach, with a spatial resolution and measurement accuracy superior to that of an SR sequence, which is poorly

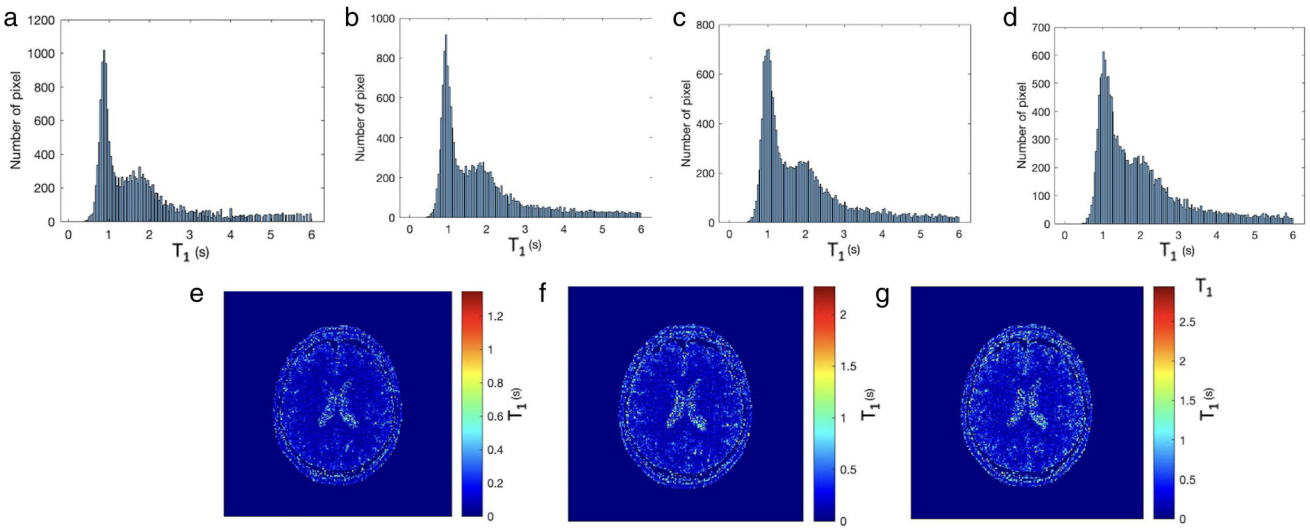

FIGURE 6: T_1 values histograms (a) from a MPRAGE-derived T_1 map in human brain (patient #1), and (b–d) after applying a randomly generated multiplier (Gaussian distribution, standard deviation (a) σ = 10%, (b) σ = 20%, and (c) σ = 30% of image signal intensity) on the proton density correction map. (e–g) Original T_1 map subtracted from the T_1 maps corresponding to histograms in (b–d).

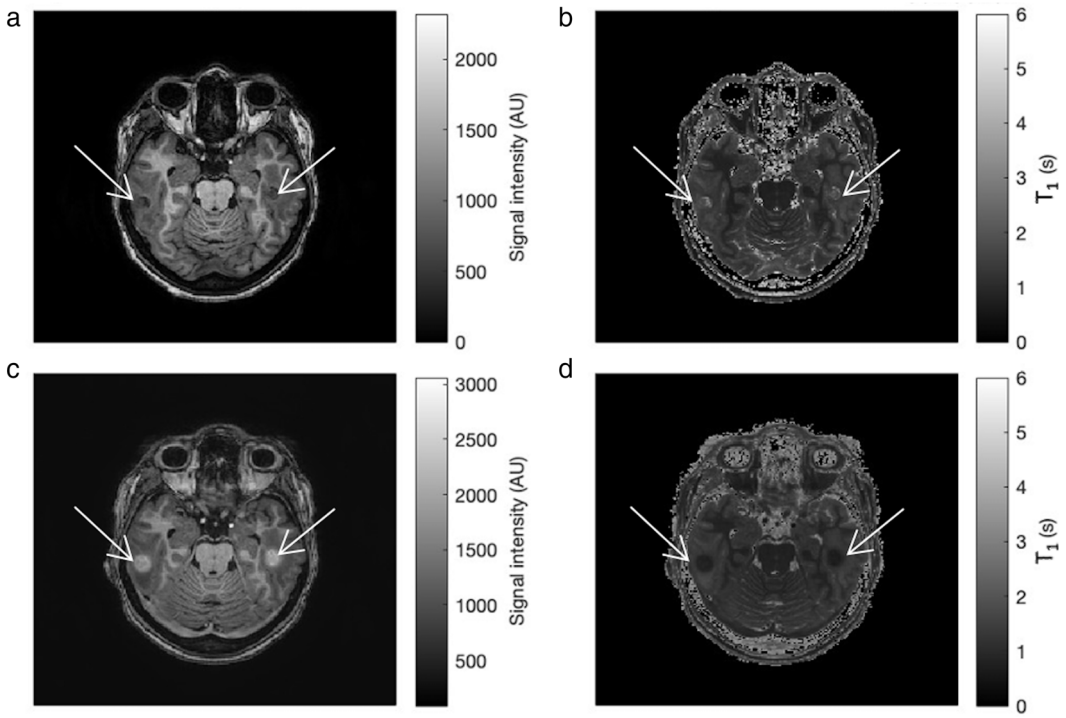

FIGURE 7: (a) MPRAGE image acquired from patient #1 and (b) corresponding T_1 map before the administration of the contrast agent. (c) MPRAGE image and (d) corresponding T_1 map 2 hours after the administration of the contrast agent. (a–d) Arrows are pointing the two brain metastases located in the right and left temporal lobes.

adapted to in vivo measurements. It should be noted once again that the acquisition times are four times lower with the 3D MPRAGE sequence compared to a single-slice acquisition SR sequence.

The T_1 measurements in the human brain also demonstrated the feasibility and accuracy of the proposed approach for the assessment of T_1 value in brain tissue. As a point of comparison the T_1 values in brain at 3 T reported in the literature are typically ranging between 0.7 and 1 seconds, 1 and 1.6 seconds, 3.8 and 5 seconds for WM, GM, and CSF, respectively.[26,33] The technique appeared less reliable for the assessment of very long T_1 such as the one found in CSF.[34] This is related to the relatively weak signal intensity from tissues with very long T_1 in MPRAGE acquisitions and to the more pronounced T_1 variations at low intensity values. In this study, the normalization of the T_1 vs. signal intensity curves was performed using a ROI in the WM. Although this normalization provided satisfactory results, it would be preferable to use an external reference with a known T_1 value.

The evaluation of the dependence of the T_1 measurements toward an inaccurate estimation of the proton density shows through the histograms that the uncertainties can be kept within acceptable limits (below 10% variations for a Gaussian standard deviation equal to 10%). The impact of T_2^* relaxation appears negligible with the sequence parameters used and the usual relaxation values in brain tissue.[27,28]

The feasibility of the approach for the measurement of the concentration of theranostic agents in a patient with brain

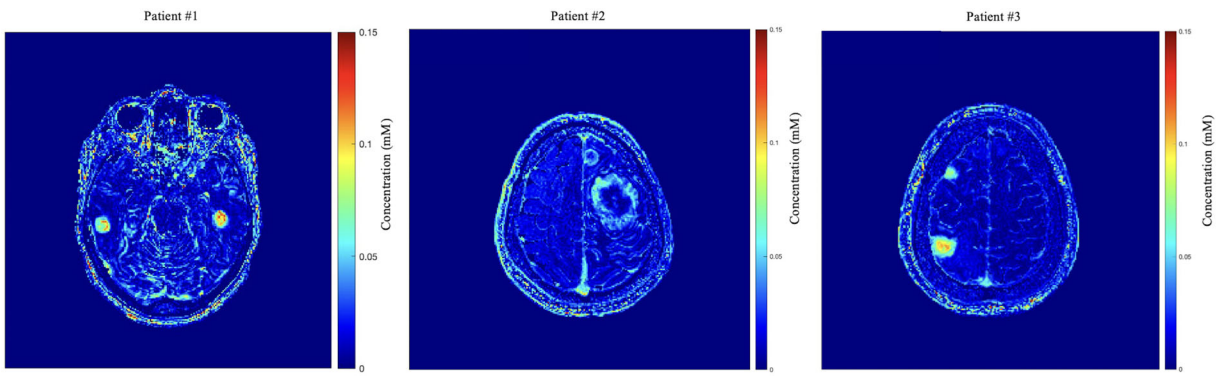

FIGURE 8: Exemplary concentration maps of the theranostic agent obtained for each of the three patients treated with AGuIX at 100 mg/kg body weight.

TABLE 2. Mean and SD of Concentration of Gd^{3+} Ion Measured in Metastases Larger Than 1-cm Diameter and in the Occipital GM Are Given for the Three Patients

Patient	Concentration of Gd^{3+} in Metastases (μM)	Concentration of Gd^{3+} in Occipital GM (μM)
1 ($N = 5$)	82.24 ± 17.55	4.34 ± 0.69
2 ($N = 10$)	44.26 ± 10.40	1.57 ± 0.12
3 ($N = 7$)	57.92 ± 12.81	3.95 ± 0.67

N corresponds to the number of metastases for each patient.

metastases was evaluated. The quantification of the concentration assumed that the known in vitro relaxivity of the contrast agents can be applied to in vivo conditions.[15,16] This assumption, applied in this study, is in all cases nonspecific to the T_1 measurement technique used. The examples of concentration maps illustrate the potential of the proposed approach to take advantage of the spatial resolution of the anatomical acquisitions of the MPRAGE sequence to finely visualize the distribution of theranostic agents in the metastases. The average concentrations measured in this proof-of-concept study on three patients are comparable to those obtained with a VFA-type sequence.[12] Yet, in the present case, a higher spatial resolution and a shortened imaging protocol of about 15 minutes for the patient could be obtained. The high spatial resolution of the MPRAGE-derived T_1 map can be used to obtain a detailed image of the heterogeneous distribution of the contrast agent in the metastases. The low concentration values measured in the occipital GM indicate the near absence of theranostic agents in healthy tissue and illustrate the validity of the computation of the concentration.

The average concentrations measured in the metastases, ranging from 36 to 97 μM of Gd^{3+}, incidentally ruled out the possibility of a decrease in the intensity of the postadministration MRI signal induced by r_2^* values of the chelated Gd ions. This is in the order of 19 mM^{-1} s^{-1} at 3 T for a Gd chelate,[35] resulting in an expected 0.8% loss of MRI signal in the metastases for a Gd^{3+} concentration of 100 μM.

The concentration measurements provided in this study may allow, in the case of theranostic agents, to 1) correlate their concentration and the magnitude of the therapeutic effect observed locally; 2) to estimate the expected therapeutic effect knowing the local concentration and consequently; and 3) to spatially adjust and intensity modulate any controllable external therapeutic modality to the local concentration of the theranostic agent. In the case of theranostic radiosensitizers such as AGuIX nanoparticles, the spatial and amplitude modulation of the ionising radiation could be carried out using standard radiotherapy equipment or MR-Linac systems.[36,37] While optimizing the irradiation of the diseased tissue with great precision, it is possible to cause as little damage as possible to the surrounding healthy tissue. This approach exemplifies the concept of personalized medicine using theranostic agents to improve cancer management by achieving maximum benefit while maintaining a high safety profile.

Even if the question of absolute concentration arises, due for example to the uncertainties on the value of the in vivo relaxivity of these agents, a measurement of their relative concentration allows to bring information on the impact of these theranostic agents in a more quantitative way than an evaluation based on signal changes in the T_1-weighted anatomical images due to the contrast agent uptake.

Limitations

A limitation of the proposed approach is its sensitivity to signal intensity variations. These intensity variations, arising for example from inhomogeneous transmit or receive profiles of the RF coils, can potentially result in a decrease in the accuracy of the measured relaxation time value. In this study, the transceiver volume coil used on the preclinical MRI scanner and the 32-channel head coil used for the clinical study help mitigate this limitation.

Conclusion

The results obtained in this study show that it is possible to estimate the concentration of contrast agents or theranostic agents using the MPRAGE sequence. Specifically, the T_1 values obtained in vitro and in vivo show that the proposed approach is valid and robust. The concentrations of Gd-based theranostic agents may be assessed in patients with metastases undergoing standard clinical imaging protocols including the MPRAGE sequence.

Acknowledgments

Audrey Lavielle was salaried by the Supermag project from innovation department of the University of Bordeaux, in the framework of IdEx Bordeaux (10-IDEX-0003), Justine Deborne was salaried by the Insight project in the framework of the Laboratory of Excellence TRAIL ANR-10-LABX-57.

References

1. Xie J, Lee S, Chen X. Nanoparticle-based theranostic agents. Adv Drug Deliv Rev 2010;62:1064-1079.
2. Mura S, Couvreur P. Nanotheranostics for personalized medicine. Adv Drug Deliv Rev 2012;64:1394-1416.
3. Bonvalot S, Le Pechoux C, De Baere T, et al. First-in-human study testing a new radioenhancer using nanoparticles (NBTXR3) activated by radiation therapy in patients with locally advanced soft tissue sarcomas. Clin Cancer Res off J Am Assoc Cancer Res 2017;23:908-917.
4. Huang HS, Hainfeld JF. Intravenous magnetic nanoparticle cancer hyperthermia. Int J Nanomedicine 2013;8:2521-2532.

5. Yan Z, Zhang X, Liu Y, et al. HSA-MnO2-131I combined imaging and treatment of anaplastic thyroid carcinoma. Technol Cancer Res Treat 2022;21:15330338221106556.
6. Verry C, Dufort S, Villa J, et al. Theranostic AGuIX nanoparticles as radiosensitizer: A phase I, dose-escalation study in patients with multiple brain metastases (NANO-RAD trial). Radiother Oncol 2021;160: 159-165.
7. Kadria-Vili Y, Neumann O, Zhao Y, et al. Gd_2O_3-mesoporous silica/gold nanoshells: A potential dual T1/T2 contrast agent for MRI-guided localized near-IR photothermal therapy. Proc Natl Acad Sci U S A 2022;119: 2123527119.
8. Muir BW, Acharya DP, Kennedy DF, et al. Metal-free and MRI visible theranostic lyotropic liquid crystal nitroxide-based nanoparticles. Biomaterials 2012;33:2723-2733.
9. Liu Y, Chen Z, Liu C, Yu D, Lu Z, Zhang N. Gadolinium-loaded polymeric nanoparticles modified with anti-VEGF as multifunctional MRI contrast agents for the diagnosis of liver cancer. Biomaterials 2011;32: 5167-5176.
10. Wang L, Xing H, Zhang S, et al. A Gd-doped Mg-Al-LDH/Au nanocomposite for CT/MR bimodal imagings and simultaneous drug delivery. Biomaterials 2013;34:3390-3401.
11. Lux F, Sancey L, Bianchi A, Crémillieux Y, Roux S, Tillement O. Gadolinium-based nanoparticles for theranostic MRI-radiosensitization. Nanomedicine 2015;10:1801-1815.
12. Verry C, Dufort S, Lemasson B, et al. Targeting brain metastases with ultrasmall theranostic nanoparticles, a first-in-human trial from an MRI perspective. Sci Adv 2020;6:eaay5279.
13. Dadfar SM, Roemhild K, Drude NI, et al. Iron oxide nanoparticles: Diagnostic, therapeutic and theranostic applications. Adv Drug Deliv Rev 2019;138:302-325.
14. Wang L, Lai S-M, Li C-Z, Yu H-P, Venkatesan P, Lai P-S. D-alpha-tocopheryl poly(ethylene glycol 1000) succinate-coated manganese-zinc ferrite nanomaterials for a dual-mode magnetic resonance imaging contrast agent and hyperthermia treatments. Pharmaceutics 2022;14: 1000-1019.
15. Haar PJ, Broaddus WC, Chen Z, Fatouros PP, Gillies GT, Corwin FD. Gd-DTPA T1 relaxivity in brain tissue obtained by convection-enhanced delivery, magnetic resonance imaging and emission spectroscopy. Phys Med Biol 2010;55:3451-3465.
16. Coolen BF, Geelen T, Paulis LEM, Nicolay K, Strijkers GJ. Regional contrast agent quantification in a mouse model of myocardial infarction using 3D cardiac T1 mapping. J Cardiovasc Magn Reson off J Soc Cardiovasc Magn Reson 2011;13:56-65.
17. Crawley AP, Henkelman RM. A comparison of one-shot and recovery methods in T1 imaging. Magn Reson Med 1988;7:23-34.
18. Look DC, Locker DR. Time saving in measurement of NMR and EPR relaxation times. Rev Sci Instrum 1970;41:250-251.
19. Stikov N, Boudreau M, Levesque IR, Tardif CL, Barral JK, Pike GB. On the accuracy of T1 mapping: Searching for common ground. Magn Reson Med 2015;73:514-522.
20. Subashi E, Choudhury KR, Johnson GA. An analysis of the uncertainty and bias in DCE-MRI measurements using the spoiled gradient-recalled echo pulse sequence. Med Phys 2014;41:032301.
21. Marques JP, Kober T, Krueger G, van der Zwaag W, Van de Moortele P-F, Gruetter R. MP2RAGE, a self bias-field corrected sequence for improved segmentation and T1-mapping at high field. Neuroimage 2010;49:1271-1281.
22. Eisenhauer EA, Therasse P, Bogaerts J, et al. New response evaluation criteria in solid tumours: Revised RECIST guideline (version 1.1). Eur J Cancer 2009;45:228-247.
23. Gowland PA, Leach MO. Fast and accurate measurements of T1 using a multi-readout single inversion-recovery sequence. Magn Reson Med 1992;26:79-88.
24. Wang J, He L, Zheng H, Lu Z-L. Optimizing the magnetization-prepared rapid gradient-Echo (MP-RAGE) sequence. PLoS One 2014;9: e96899.
25. Ting Y-L, Bendel P. Thin-section MR imaging of rat brain at 4.7 T. J Magn Reson Imaging 1992;2:393-399.
26. Hagiwara A, Fujimoto K, Kamagata K, et al. Age-related changes in relaxation times, proton density, myelin, and tissue volumes in adult brain analyzed by 2-dimensional quantitative synthetic magnetic resonance imaging. Invest Radiol 2021;56:163-172.
27. Cohen-Adad J. What can we learn from T2* maps of the cortex? Neuroimage 2014;93:189-200.
28. Péran P, Hagberg G, Luccichenti G, et al. Voxel-based analysis of R2* maps in the healthy human brain. J Magn Reson Imaging 2007;26: 1413-1420.
29. Vayssières L, Chanéac C, Tronc E, Jolivet JP. Size tailoring of magnetite particles formed by aqueous precipitation: An example of thermodynamic stability of nanometric oxide particles. J Colloid Interface Sci 1998;205:205-212.
30. Adumeau L, Genevois C, Roudier L, Schatz C, Couillaud F, Mornet S. Impact of surface grafting density of PEG macromolecules on dually fluorescent silica nanoparticles used for the in vivo imaging of subcutaneous tumors. Biochim Biophys Acta Gen Subj 2017;1861:1587-1596.
31. Lux F, Mignot A, Mowat P, et al. Ultrasmall rigid particles as multimodal probes for medical applications. Angew Chem Int Ed Engl 2011;50: 12299-12303.
32. Deruelle T, Kober F, Perles-Barbacaru A, et al. A multicenter preclinical MRI study: Definition of rat brain relaxometry reference maps. Front Neuroinform 2020;14:22.
33. Shin W, Gu H, Yang Y. Fast high-resolution T1 mapping using inversion-recovery Look-Locker echo-planar imaging at steady state: Optimization for accuracy and reliability. Magn Reson Med 2009;61: 899-906.
34. Bojorquez JZ, Bricq S, Acquitter C, Brunotte F, Walker PM, Lalande A. What are normal relaxation times of tissues at 3 T? Magn Reson Imaging 2017;35:69-80.
35. Patil V, Johnson G. ΔR2 (*) gadolinium-diethylenetriaminepentacetic acid relaxivity in venous blood. Magn Reson Med 2013;69:1104-1108.
36. Randall JW, Rammohan N, Das IJ, Yadav P. Towards accurate and precise image-guided radiotherapy: Clinical applications of the MR-Linac. J Clin Med 2022;11:4044-4061.
37. Werensteijn-Honingh AM, Kroon PS, Winkel D, et al. Impact of magnetic resonance-guided versus conventional radiotherapy workflows on organ at risk doses in stereotactic body radiotherapy for lymph node oligometastases. Phys Imaging Radiat Oncol 2022;23:66-73.